An improved setup for radial diffraction experiments at high pressures and high temperatures in a resistive graphite-heated diamond anvil cell

Julia Immoor, Hauke Marquardt, Lowell M Miyagi, S. Speziale, Sébastien Merkel, I. Schwark, A. Ehnes, Hanns-Peter Liermann

Review of Scientific Instruments

An improved setup for radial diffraction experiments at high pressures and high temperatures in a resistive graphite-heated diamond anvil cell.

J. Immoor[1], H. Marquardt[2], L. Miyagi[3], S. Speziale[4], S. Merkel[5], I. Schwark[6], A. Ehnes[6], H.-P. Liermann[6]

[1]Bayerisches Geoinstitut BGI, University of Bayreuth, 95440 Bayreuth, Germany; [2]Department of Earth Sciences, University of Oxford, Oxford OX1 3AN, UK; [3]University of Utah, 115 So. 1460 E., Salt Lake City, UT84112-0111, USA; [4]German Research Center for Geosciences GFZ, 14473 Potsdam, Germany; [5]Univ. Lille, CNRS, INRAE, Centrale Lille, UMR 8207 - UMET - Unité Matériaux et Transformations, F-59000 Lille, France; [6]Photon Sciences, Deutsches Elektronen-Synchrotron (DESY), 22607 Hamburg, Germany

*Correspondence to: Julia.immoor@uni-bayreuth.de

Abstract

We present an improved setup for the experimental study of deformation of solids at simultaneous high pressures and temperatures by radial X-ray diffraction. The technique employs a graphite resistive heated Mao Bell type diamond anvil cell (DAC) for radial X-ray diffraction in combination with a water-cooled vacuum chamber. The new chamber has been developed by the sample environment group at PETRA III and implemented at the Extreme Conditions Beamline (ECB) P02.2 at PETRA III, DESY (Hamburg, Germany). We discuss applications of the new setup to study deformation of a variety of materials, including ferropericlase, calcium perovskite, bridgmanite, and tantalum carbide at high-pressure/temperature.

Introduction

Understanding the physical and rheological properties of materials at simultaneous high pressures and temperatures is of key importance in Earth science as well as materials sciences. The rheological properties of Earth's mantle materials, for example, govern large-scale mantle convection[1–4]. In addition, Crystallographic Preferred Orientation (CPO) caused by the alignment of mantle minerals during deformation, leads to seismic anisotropy, providing a means to link seismic observations to mantle flow[5–13]. Several techniques have been developed in the past to study the rheology of materials under high pressure and temperature, but achievable pressures are mostly limited to those typical of the crust and upper mantle[3,14–18].

Deformation experiments at deep lower mantle pressures are almost exclusively performed in diamond-anvil cells in combination with synchrotron-based in-situ X-ray diffraction in a radial geometry (Fig. 1A, B). By employing radial diffraction geometry, lattice strains and deviatoric stress as well as evolution of CPO can be derived from analysis of in situ diffraction images. Radial X-ray diffraction in DACs has been widely employed in Earth as well as materials sciences, but high-pressure experiments have been mostly limited to room temperature[19–25]. Early high-temperature employed a laser-heated DAC, but data analysis and interpretation is challenging due to temperature gradients in the sample[26,27]. Liermann *et al.*, (2009)[28] developed a resistive-heated DAC, which was tested up to 36 GPa and 1100 K while performing in-situ radial X-ray diffraction. The use of a resistive-heating setup reduces temperature gradients and provides more homogeneous heating of the entire sample chamber.

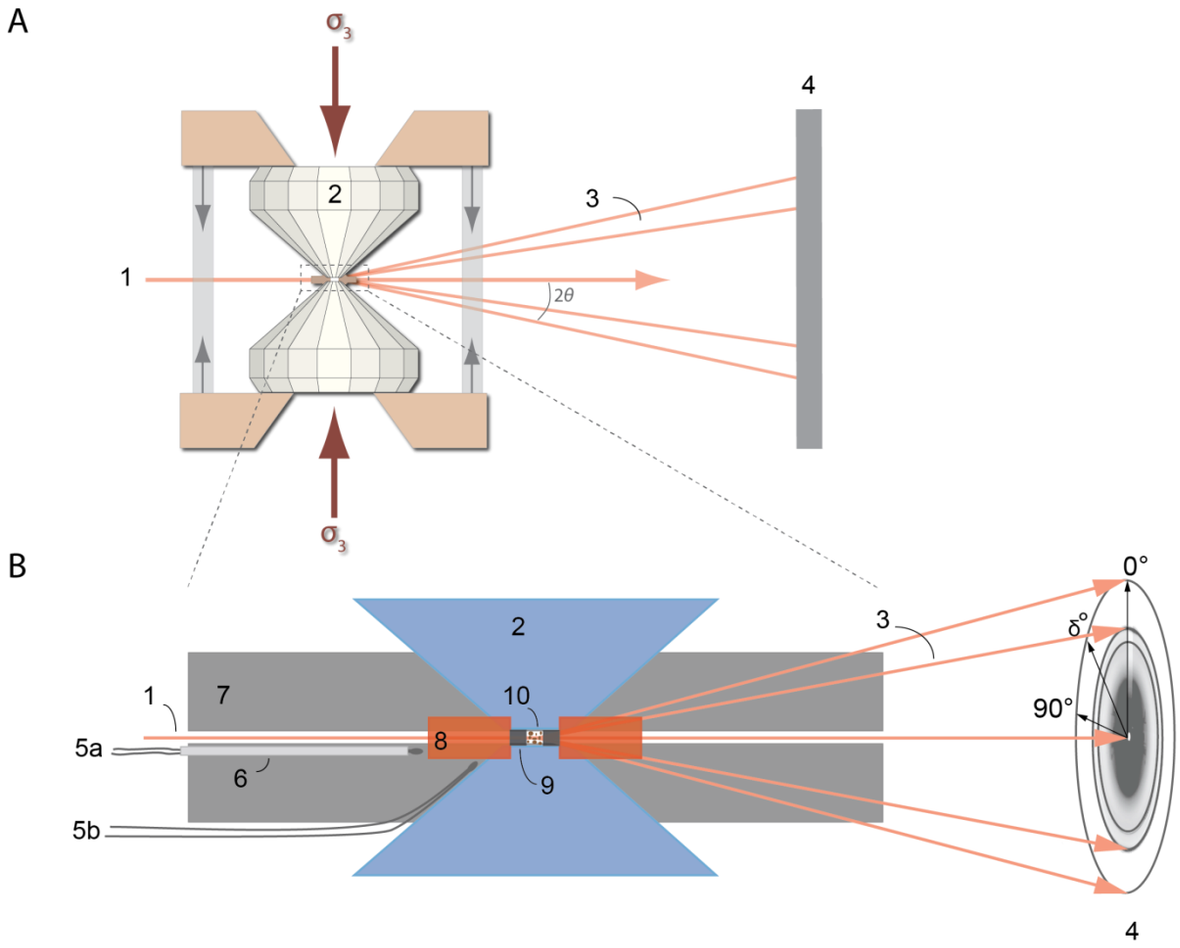

Figure 1: (A) angle-dispersive high-pressure radial X-ray diffraction in a DAC (modified after [28]); σ_3: stress along compression direction; 2θ: diffraction angle; 1: incoming X-ray Beam; 2: Diamond anvil; 3: Diffracted beam; 4: Area detector. (B) Magnification of the diamond-anvil culets showing the position for the two thermocouples (5a: between both graphite heaters; 5b: on the diamond anvil next to the culet). 6: Ceramic sleeve; 7: Flexible graphite sheet; 8: Kapton; 9: Boron gasket; 10: sample.

Here, we present a modified resistive-heated-radial-X-ray-diffraction-diamond-anvil-cell (RH-rXRD-DAC) (Fig. 2A, B) and report on its performance during in-situ radial X-ray diffraction experiments at simultaneous high pressure and high temperature on several

Review of Scientific Instruments

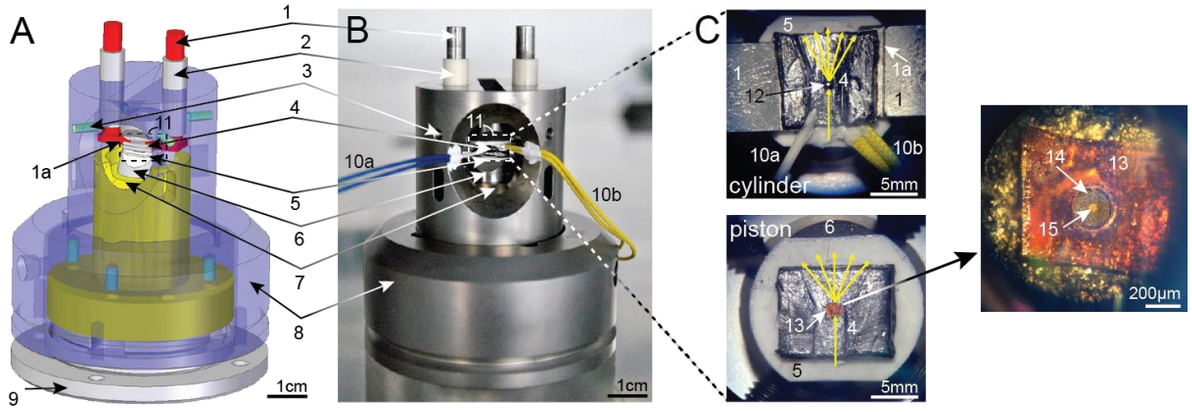

Figure 2: Experimental setup of a resistive-heated DAC (modified after[10]). (A) 3D CAD model and (B) photograph of the resistive-heated DAC used for the experiments. 1: Molybdenum rods (electrical contacts); 1a: Strip with step at the end of molybdenum rod; 2: Ceramic sleeves; 3: Screws; 4: Graphite sheet; 5: Ceramic plate; 6: Tungsten carbide seat; 7: Piston; 8: Cylinder; 9: Membrane cup (missing in B); 10a: Thermocouple with ceramic sleeve; 10b: Thermocouple; 11: Graphite-heater. (C) Close-up of 11. Cylinder: 12: Culet of a diamond; 4: Flexible graphite sheet with carved space for X-ray beam. Inset shows the lower diamond pressed into the graphite heater and illustrates the positions of the thermocouples. Piston: 13: Kapton, which supports a cubic boron nitride gasket or amorphous boron epoxy gasket (14) with powder sample in the sample chamber (15).

polycrystalline samples. The main improvement as compared to the setup described by Liermann et al. (2009) is the development and implementation of a water-cooled vacuum chamber (Fig. 3A, B) that also enables cooling of the piston of the Mao Bell type DAC. This modification decreases heating and thermal expansion of the piston of the Mao Bell DAC but allows the cylinder to heat up, thus reducing friction between the piston and the cylinder during compression at high temperatures. The use of a vacuum chamber prevents the oxidation of the cell, the Molybdenum rods and the diamonds at very high temperatures. We

discuss applications of the improved setup for studying the deformation behavior of major materials expected in Earth's lower mantle as well as tantalum carbide.

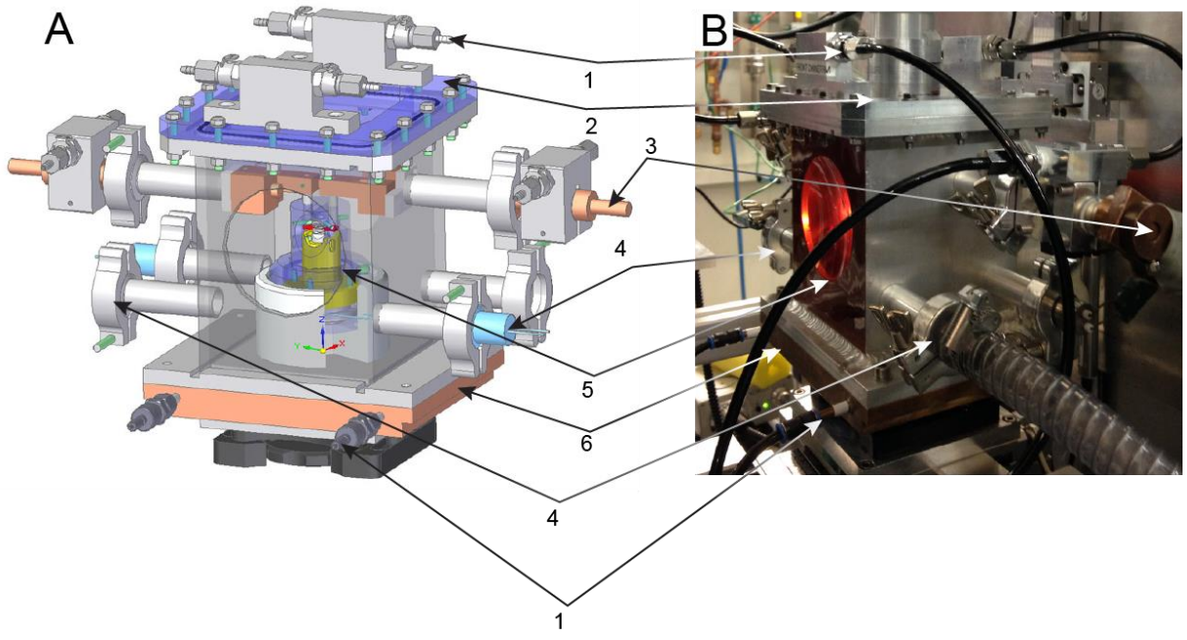

Figure 3: (A) 3D CAD model of the vacuum chamber. (B) Photograph of the vacuum chamber while performing a high-temperature experiment (~1400 K). 1: Water cooling inlet/outlet; 2: Lid with screws; 3: Power supply connector; 4: Vacuum pump connection; 5: Kapton window; 6: Copper cooling plate.

Experimental Method

In radial X-ray diffraction experiments, the incoming X-ray beam is oriented perpendicular to the compression direction, i.e. the axis of the diamond anvils (Fig. 1A, C: 1). This setup provides the possibility to study the lattice strains, resulting from the effect of differential stress, together with the CPO of powder samples[19]. A pressure-transmitting medium is not used. This enhances the development of differential stress and texture. In order for X-rays to reach the sample chamber in the radial diffraction geometry, X-ray transparent gaskets are required. Here, we used either X-ray transparent amorphous boron epoxy + kapton[29] or cubic boron nitride (cBN) epoxy[27] (10:1 Epotech 353ND) + kapton gaskets (Fig. 1: 8, 9; Fig. 2C:

13, 14) to reach high pressures[30]. The culet sizes of the employed diamonds were 200 µm or 300 µm (Fig. 2C: 12). The setup of the graphite heater is similar on the piston and cylinder side of the DAC (Fig. 2C). Diamonds are glued on tungsten carbide seats that are truncated at the side to increase the opening angle for diffracted X-rays (Fig. 2: 5). The seats are insulated from the graphite by a ceramic ring (Fig. 2: 4) fixed to the seat with OMEGABOND 500 liquid. The gaps between the ceramic plates and the diamonds are filled with ceramic glue (Resbond 989). The heads of the molybdenum rods end in horizontal strips with a small step at the end. A piece of graphite foil connects the molybdenum rods (Fig. 2A: 1a; Fig. 2B: 11; Fig. 2C: 1a) and serves as heating element surrounding the diamond-anvils. A space is carved in the graphite foil to prevent diffraction of the graphite contaminating the diffraction image. Two thermocouples (R-type) are attached to the cylinder side. One thermocouple is placed close to the tip of the diamond on the upstream side of the DAC and to the side of the path of the incident X-ray beam (Fig 2C: 10a). The second thermocouple is positioned on the graphite sheet, likewise upstream and to the side of the incident X-ray beam (Fig. 2C: 10b). When the cell is closed, the second thermocouple rests between the graphite sheets of the piston and the cylinder.

During the experiment, the temperature of the sample can be increased/decreased by varying an analog I/O signal from 0-10 V using the beamline control system. This proportionally adjusts the power of the DC power supply from 0-1800 W (0–8 V and 0–220 A)[31]. Pressure is changed remotely using a gas membrane device that is operated by the membrane pressure controller APD200 from Sanchez Technology[27,28,32].

For high-pressure and high-temperature experiments, the RH-rXRD-DAC is placed in a newly-designed water-cooled vacuum chamber that serves to both cool the DAC and to prevent oxidation of the DAC, the molybdenum electrodes, the diamond anvils and the graphite heater (Fig. 3A, B). The piston of the DAC is indirectly cooled through a steel pin

that is connected to the base of the vacuum chamber, which is water-cooled. The differential cooling between the piston and the cylinder reduces the friction between the two parts of the DAC and enables a smoother pressure increase as compared to the previous experimental setup[27,28]. During the experiment the vacuum in the chamber can be as good as 5 x 10^{-3} mbar. Note that, due to connections between the pump and the cell chamber, vacuum levels around the diamond anvil cells may not be as efficient. Nevertheless, the achieved vacuum is sufficient to perform experiments with minimal oxidation of the heating elements.

Results and discussion

The new setup has been tested during different experimental campaigns at the ECB P02.2 at PETRA III, DESY (Hamburg, Germany). Diffraction images were collected with a XRD 1621 flat panel detector from Perkin Elmer. In the following, we will describe some selected experiments in order to illustrate the capability of the new setup for Earth and materials science research. We report on the deformation of polycrystalline samples of ferropericlase ($(Mg_{0.8}Fe_{0.2})O$), the in-situ synthesis and deformation of cubic Ca-Pv ($CaSiO_3$), experiments performed on a two-phase mixture of bridgmanite ($MgSiO_3$) and ferropericlase, synthesized from a mixture of enstatite glass + ferropericlase in the resistive-heated DAC, as well as the high-temperature compression of tantalum carbide ($TaC_{0.99}$), an ultra-high temperature ceramic material.

1. In-situ deformation of ferropericlase

Ferropericlase is the second most abundant mineral in Earth's lower mantle. It may play a key role in mantle dynamics since it is rheologically weaker than bridgmanite, the dominant lower mantle phase. Furthermore, it shows a pronounced elastic anisotropy, making it one of the candidates to explain seismic shear wave polarization anisotropy in the lower mantle[33].

143 However, previous deformation studies at pressures of the lower mantle were limited to room
144 temperature due to experimental complexity[19,21–23,34,35]. In Immoor *et al.* (2018), we used the
145 described setup to measure the deformation of ferropericlase to 62 GPa at 1400 K as well as
146 to higher pressures but lower temperature. In our 1400 K run, the pressure of the sample was
147 increased up to 40 GPa at room temperature and afterwards heated up to 1400 K. During
148 heating, the pressure of the sample dropped to below 20 GPa. We increased the pressure again
149 and reached 62 GPa when diamond failure stopped the experiment. During compression, we
150 collected high quality diffraction images of ferropericlase. Based on these results, we were
151 able to monitor the evolution of CPO in ferropericlase and confirm a change of slip system
152 activity at high temperature as predicted by computations[10].
153
154 *2. In-situ synthesis and deformation of cubic $CaSiO_3$*
155 $CaSiO_3$ perovskite is expected to be an important mineral in Earth's transition zone and lower
156 mantle, where it is the third most abundant phase for a pyrolytic mantle composition[36]. In a
157 deeply subducted oceanic slab, $CaSiO_3$ perovskite may account for up to 25 Vol.% of the
158 transformed basaltic crust[37] and will affect the bulk rheological properties of the lithospheric
159 slab. According to a recent computational study[38], the shear wave anisotropy of $CaSiO_3$
160 perovskite is about 15-30% at conditions of the lower mantle. A strong CPO of $CaSiO_3$
161 perovskite may, therefore, contribute to seismic anisotropy observations, in particular in the
162 shallow lower mantle or lowermost transition zone, where the elastic anisotropy is strongest.
163 A previous $CaSiO_3$ perovskite study has been limited to 49 GPa at ambient conditions[23]. At
164 these conditions, however, $CaSiO_3$ perovskite forms a pseudo cubic structure and the exact
165 nature of the distortion is still under debate[39–42]. Whereas at temperatures typical for the lower
166 mantle, the structure is cubic ($Pm3m$)[40–43] and may show a different rheological behavior.
167 $CaSiO_3$ perovskite can be experimentally synthesized from $CaSiO_3$ wollastonite at pressures

of about 20 GPa and temperature of about 1300 K[44], but is not quenchable to ambient conditions. This implies that studies of the physical properties of $CaSiO_3$ perovskite need to be performed in-situ and in the same pressure device where it has been synthesized.

Using the improved RH-rXRD-DAC, we were able to synthesize $CaSiO_3$ perovskite and performed several successful deformation experiments reaching temperatures of up to 1500 K at pressures of 45 GPa (Immoor *et al.* in prep.). The starting material was amorphous $CaSiO_3$ mixed with platinum powder as pressure standard. Figure 4 shows two diffraction images collected during a compression experiment that reached a final pressure of 40 GPa at 1300 K. Cubic $CaSiO_3$ perovskite was synthesized after increasing the temperature to 1300 K at which point the pressure dropped from 33 GPa to 27 GPa as a result of the phase transition (Fig. 4B). The collected diffraction patterns show smooth diffraction rings, indicating a relatively small and homogeneous grain size of the synthesized cubic $CaSiO_3$ perovskite. The large pressure drop at the transition also caused strain heterogeneity in Pt finely mixed with the sample (see Pt peaks asymmetry in Fig. 4B).

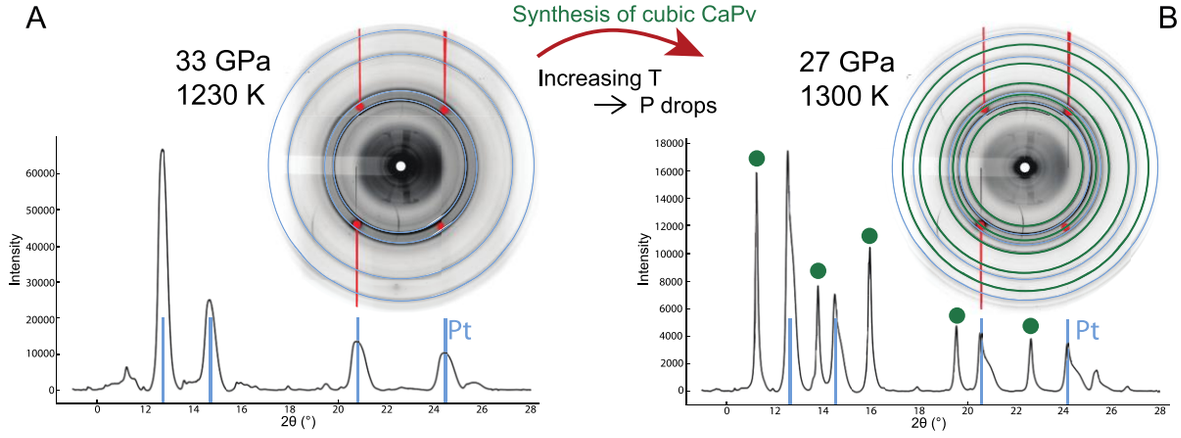

Figure 4: Synthesis of cubic calcium perovskite. The pressure was calculated from the stronger Pt peak. (A) X-ray diffraction image at 33 GPa and 1230 K shows rings of Pt (blue), which are used to estimate the pressure during the experiment and diamond single-crystal diffraction spots (red). The corresponding integrated diffraction pattern is shown below with

blue line indicating Pt peaks. (B) X-ray diffraction image at 27 GPa and 1300 K with Debye rings of Pt (blue), Debye rings of calcium perovskite (green) and diamond diffraction spots (red). At the bottom integrated diffraction pattern with blue lines indicating Pt peaks and green dots indicating calcium perovskite peaks.

In both panel (A) and (B) the diffraction lines of diamond are masked in the integration and absent in the diffraction patterns.

3. Synthesis of Bridgmanite and Ferropericlase

The deformation behavior of multiphase rock assemblies might substantially differ from the behavior of single-phase assemblies, particularly if the phases show large differences in rheological properties [35,45–48]. The lower mantle can be modeled as a two-phase mixture of bridgmanite and ferropericlase, two phases that show large differences in plastic strength and viscosity[3,5,22]. Because of this large contrast in rheological strength, it is difficult to predict mantle properties, including viscosity and seismic anisotropy, from single-phase measurements. There have been few deformation experiments on analogues[49,50], as well as on a true two-phase lower mantle mixture at pressures and temperature of the very top of the lower mantle using a rational Drickamer apparatus[3]. Here, we used the improved RH-rXRD-DAC to synthesize a bridgmanite and ferropericlase assembly (Fig. 5A, B) from an enstatite glass powder mixed with ferropericlase, and applied deviatoric stress to the two-phase mixture at high temperatures (Fig. 5C). In one successful run, we first increased the pressure at 1600 K. Afterwards the pressure in the sample decreased while increasing the temperature continuously to 1900 K. A peak splitting of ferropericlase was observed, likely as a result of pressure gradients in the sample chamber, followed by the appearance of the typical diffraction ring triplet of the new phase bridgmanite. Bridgmanite grew while the pressure continued to decrease when the thermocouples stopped working. During a subsequent

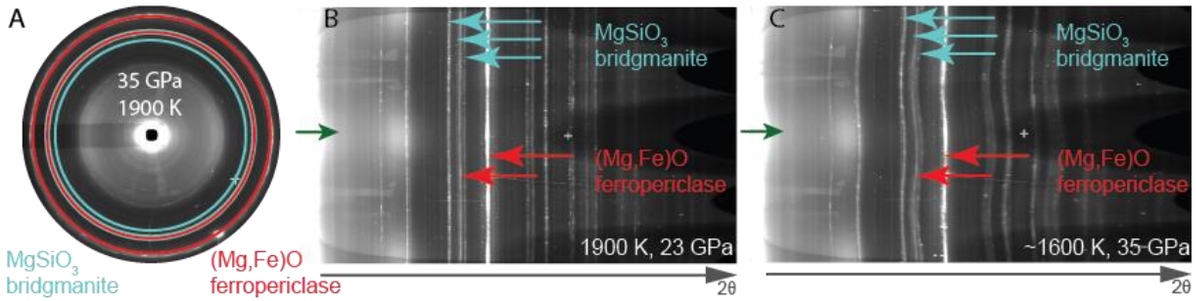

Figure 5: Synthesis of bridgmanite (blue) + ferropericlase (red). Green arrows indicate the compression direction in the unrolled radial X-ray diffraction image. (A) shows the diffraction rings of bridgmanite and ferropericlase at 35 GPa and 1900 K. (B) shows the unrolled image with the straight unrolled diffraction rings of bridgmanite and ferropericlase at 23 GPa and 1900 K. (C) The unrolled diffraction image shows the curved unrolled diffraction rings of bridgmanite and ferropericlase after pressure increase up to 35 GPa at ~1600 K. Ferropericlase was used as pressure calibrant.

decrease of voltage and therefore presumably of temperature (based on power-temperature relation; see Fig. 6), the pressure in the sample chamber increased again to 35 GPa leading to deformation of the sample (Fig. 5C).

4. Compression of tantalum carbide ($TaC_{0.99}$)

Carbides are characterized by high mechanical and thermal stability and play an important role in industrial applications, where they are used, for example, as coatings for abrasive tools. Many experimental and computational studies have been conducted on tantalum carbide (see references in[51]). However, no experiments have been performed to study the behavior of this phase under simultaneous high pressure, high temperature and deviatoric stress. We performed two successful experimental deformation runs on tantalum carbide ($TaC_{0.99}$) and constrained the pressure-volume-temperature equation of state[51]. The starting material was

233 $TaC_{0.99}$ powder and the pressure was determined by a thin piece of Au foil (less than 5 µm)
234 using the EOS published in Fei et al. (2007). In the first run, we started heating when the
235 pressure reached 2 GPa, we increased the temperature to 673 K, and measured X-ray
236 diffraction up to a final pressure of 33 GPa along the 673 K isotherm. In the second run, we
237 increased temperature at a pressure of ~2 GPa up to 1073 K, and we collected X-ray
238 diffraction images up to a final pressure of ~38 GPa along an isothermal path. The data
239 collected under non-hydrostatic conditions were used to constrain the quasi-hydrostatic high
240 temperature EOS by extracting the hydrostatic unit-cell parameter from the x-ray diffraction
241 data[53]. In addition these data can be used to determine the strength and activity of the slip
242 systems of $TaC_{0.99}$ at simultaneous high-pressure and -temperature (Speziale *et al.* in prep.).
243
244 *5. Challenges and solutions*
245 In several experimental runs the DAC jammed during high-temperature experiments leading
246 to discrete pressure jumps as opposed to smooth increases of pressure. Because of their
247 brittleness the ceramic gaskets were not able to buffer these pressure jumps resulting in failure
248 of the diamond anvils. The reason for our difficulties to smoothly increase pressure at very
249 high temperatures could be the expansion of both the piston and the cylinder of the Mao Bell
250 DAC leading to increased friction between both parts. However, at moderately high
251 temperatures, up to 1400 K, the differential cooling was effective such that a smooth pressure
252 increase is generally possible. For higher temperature experiments the indirect piston cooling
253 is still insufficient, and needs to be improved in order to reduce the thermal expansion of the
254 piston and thus the friction.
255 Using the water-cooled vacuum chamber, temperatures up to 1900 K have been reached in the
256 RH-rXRD-DAC, but no pressure increase was possible. Generally, both thermocouples

recorded stable temperatures during the experiments, with a reproducible dependence of temperature on power (Fig. 6).

In a few runs, the difference in temperature reading between the two thermocouples was very large (the maximum difference observed was 400 K). In these cases higher temperature values were recorded by the thermocouple situated between the graphite sheets. Large differences in temperature reading usually occurred when one of the thermocouples, i.e. the one at the tip of the diamond was placed too far from the culet of the diamond.

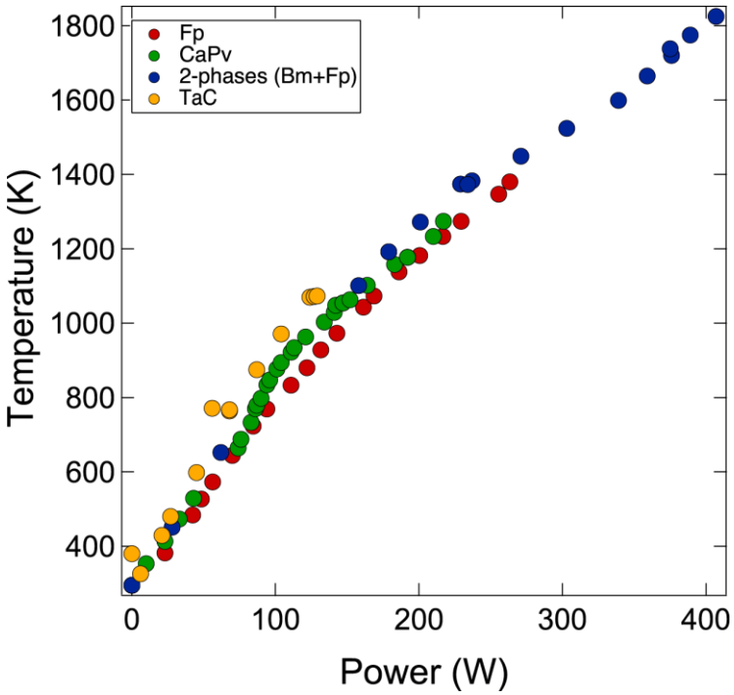

Figure 6: Power – Temperature curves of different experiments. The temperature is read using two thermocouples, one placed between the two graphite heaters and one placed on the diamond-anvil close to the sample. Symbols: Fp is ferropericlase; CaPv is calcium perovskite; Bm is bridgmanite; TaC is tantalum carbide.

Conclusion

We have presented an improved experimental setup for radial X-ray diffraction measurements based on a graphite-heated Mao Bell type diamond-anvil cell contained in a water-cooled

vacuum chamber. The setup is available for users at the Extreme Conditions Beamline P02.2 at DESY, Hamburg and allows for reaching temperatures of up to 1900 K at high pressures (Fig. 7).

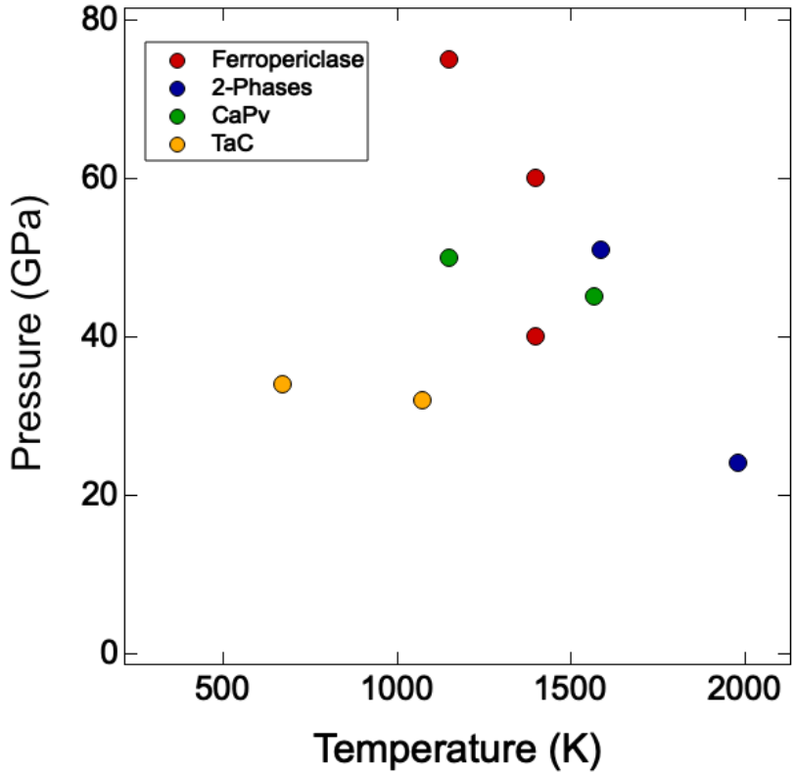

Figure 7: Maximum pressure-temperature- conditions reached in experiments on ferropericlase (red, calculated pressure), 2-phases (enstatite (bridgmanite) + ferropericlase) (blue, estimated pressure), calcium perovskite CaPv (green, 45 GPa estimated pressure; 50 GPa calculated pressure) and tantalum carbide TaC (yellow, calculated pressure) in different experimental runs.

Temperature and pressure in the diamond-anvil cell are controlled remotely during the experiment. Several successful experiments studies were performed by using the improved setup on a variety of Earth materials (ferropericlase, calcium perovskite, a two-phase bridgmanite-ferropericlase mixture) and tantalum carbide in order to show the capabilities of the resistive-heated-radial-X-ray-diffraction-diamond-anvil-cell. A major priority is currently

287 the search for a better gasket material which combines mechanical strength and high-
288 temperature stability.

289

290 Acknowledgements

291 This research was supported through the projects “GeoMaX” funded under the Emmy-
292 Noether Program of the German Science Foundation (MA4534/3-1) as well as grant
293 MA4534/4-1. HM acknowledges support from the Bavarian Academy of Sciences. LM
294 acknowledges support from the US Department of Energy, National Nuclear Security
295 Administration, through the Capital-DOE Alliance Center (DE-NA0003858) and NSF (EAR-
296 1344579 and EAR-1654687). SM acknowledges support from the Institut Universitaire de
297 France and the program PNP of CNRS/INSU. We acknowledge DESY (Hamburg, Germany),
298 a member of the Helmholtz Association HGF, for the provision of experimental facilities.
299 Parts of this research were carried out at PETRA III and we would like to thank K. Glazyrin
300 for assistance in using Beamline P02.2. Part of the research leading to this result has been
301 supported by the project CALIPSO plus under the Grant Agreement 730872 from the EU
302 Framework Programme for Research and Innovation HORIZON 2020.

303

304 References

305 [1] D.L. Kohlstedt, *Properties of Rocks and Minerals - Constitutive Equations, Rheological*
306 *Behavior, and Viscosity of Rocks* (Elsevier B.V., 2007).
307 [2] N. Tsujino, Y. Nishihara, D. Yamazaki, Y. Seto, Y. Higo, and E. Takahashi, Nature 539, 81
308 (2016).
309 [3] J. Girard, G. Amulule, R. Farla, A. Mohiuddin, and S. Karato, Science. 351, 144 (2016).
310 [4] S. Karato and P. Wu, Science. 260, 771 (1993).
311 [5] D. Yamazaki and S. Karato, Am. Mineral. 86, 385 (2001).
312 [6] B. Romanowicz and H.R. Wenk, Phys. Earth Planet. Inter. 269, 58 (2017).
313 [7] P.J. Tackley, Science. 288, 2002 (2000).
314 [8] S. Karato, Phys. Earth Planet. Inter. 51, 107 (1988).
315 [9] S. Karato, S. Zhang, and H.-R. Wenk, Science. 270, 458 (1995).
316 [10] J. Immoor, H. Marquardt, L. Miyagi, F. Lin, S. Speziale, S. Merkel, J. Buchen, A.
317 Kurnosov, and H.P. Liermann, Earth Planet. Sci. Lett. 489, 251 (2018).
318 [11] N. Creasy, M.D. Long, and H.A. Ford, J. Geophys. Res. Solid Earth 122, 5243 (2017).
319 [12] C.P. Conrad, M.D. Behn, and P.G. Silver, J. Geophys. Res. Solid Earth 112, 1 (2007).
320 [13] A. Nowacki, A.M. Walker, J. Wookey, and J.M. Kendall, Geophys. J. Int. 192, 1085
321 (2013).
322 [14] T. Kawazoe, N. Nishiyama, Y. Nishihara, T. Irifune, D. Suetsugu, C. Bina, T. Inoue, D.
323 Wiens, and M. Jellinek, Phys. Earth Planet. Inter. 183, 190 (2010).
324 [15] Y. Wang, W.B. Durham, I.C. Getting, and D.J. Weidner, Rev. Sci. Instrum. 74, 3003
325 (2003).
326 [16] D. Yamazaki and S.-I. Karato, Rev. Sci. Instrum. 72, 4207 (2001).
327 [17] T. Kawazoe, T. Ohuchi, Y. Nishihara, N. Nishiyama, K. Fujino, and T. Irifune, Phys. Earth
328 Planet. Inter. 216, 91 (2013).

[18] S.A. Hunt and D.P. Dobson, Rev. Sci. Instrum. 88, (2017).

[19] H.-R. Wenk, I. Lonardelli, S. Merkel, L. Miyagi, J. Pehl, S. Speziale, and C.E. Tommaseo, J. Phys. Condens. Matter 18, S933 (2006).

[20] S. Merkel, J. Phys. Condens. Matter 18, S949 (2006).

[21] C.E. Tommaseo, J. Devine, S. Merkel, S. Speziale, and H.R. Wenk, Phys. Chem. Miner. 33, 84 (2006).

[22] H. Marquardt and L. Miyagi, Nat. Geosci. 8, 311 (2015).

[23] L. Miyagi, S. Merkel, T. Yagi, N. Sata, Y. Ohishi, and H.R. Wenk, Phys. Earth Planet. Inter. 174, 159 (2009).

[24] H.-R. Wenk, J.R. Baumgardner, R.A. Lebensohn, and C.N. Tomé, J. Geophys. Res. Solid Earth 105, 5663 (2000).

[25] S. Merkel, A.K. McNamara, A. Kubo, S. Speziale, L. Miyagi, Y. Meng, T.S. Duffy, and H.R. Wenk, Science. 316, 1729 (2007).

[26] M. Kunz, W. a Caldwell, L. Miyagi, and H.-R. Wenk, Rev. Sci. Instrum. 78, 063907 (2007).

[27] L. Miyagi, W. Kanitpanyacharoen, S.V. Raju, P. Kaercher, J. Knight, A. MacDowell, H.R. Wenk, Q. Williams, and E.Z. Alarcon, Rev. Sci. Instrum. 84, 025118 (2013).

[28] H.-P. Liermann, S. Merkel, L. Miyagi, H.-R. Wenk, G. Shen, H. Cynn, and W.J. Evans, Rev. Sci. Instrum. 80, 104501 (2009).

[29] S. Merkel and T. Yagi, Rev. Sci. Instrum. 76, 2005 (2005).

[30] N. Funamori and T. Sato, Rev. Sci. Instrum. 79, 1 (2008).

[31] H.P. Liermann, Z. Konôpková, W. Morgenroth, K. Glazyrin, J. Bednarčik, E.E. McBride, S. Petitgirard, J.T. Delitz, M. Wendt, Y. Bican, A. Ehnes, I. Schwark, A. Rothkirch, M. Tischer, J. Heuer, H. Schulte-Schrepping, T. Kracht, and H. Franz, J. Synchrotron Radiat. 22, 908 (2015).

354 [32] S. Merkel, H.-P. Liermann, L. Miyagi, and H.-R. Wenk, Acta Mater. 61, 5144 (2013).

355 [33] H. Marquardt, S. Speziale, H.J. Reichmann, D.J. Frost, F.R. Schilling, and E.J. Garnero,
356 Science. 324, 224 (2009).

357 [34] J.-F. Lin, H.-R. Wenk, M. Voltolini, S. Speziale, J. Shu, and T.S. Duffy, Phys. Chem.
358 Miner. 36, 585 (2009).

359 [35] S. Merkel, J. Geophys. Res. 107, (2002).

360 [36] D. Frost, Elements 4, 171 (2008).

361 [37] T. Irifune and T. Tsuchiya, in *Treatise Geophys. Second Ed.* (2015).

362 [38] K. Kawai and T. Tsuchiya, Geophys. Res. Lett. 42, 2718 (2015).

363 [39] S.-H. Shim, R. Jeanloz, and T.S. Duffy, Geophys. Res. Lett. 29, 2166 (2002).

364 [40] R. Caracas, R. Wentzcovitch, G.D. Price, and J. Brodholt, Geophys. Res. Lett. 32, 1 (2005).

365 [41] D.Y. Jung and A.R. Oganov, Phys. Chem. Miner. 32, 146 (2005).

366 [42] D.J. Adams and A.R. Oganov, Phys. Rev. B - Condens. Matter Mater. Phys. 73, 1 (2006).

367 [43] T. Komabayashi, K. Hirose, N. Sata, Y. Ohishi, and L.S. Dubrovinsky, Earth Planet. Sci.
368 Lett. 260, 564 (2007).

369 [44] T. Uchida, Y. Wang, N. Nishiyama, K. ichi Funakoshi, H. Kaneko, A. Nozawa, R.B. Von
370 Dreele, M.L. Rivers, S.R. Sutton, A. Yamada, T. Kunimoto, T. Irifune, T. Inoue, and B. Li,
371 Earth Planet. Sci. Lett. 282, 268 (2009).

372 [45] M.R. Handy, J. Struct. Geol. 16, 287 (1994).

373 [46] S. Karato, Phys. Earth Planet. Inter. 24, 1 (1981).

374 [47] Y.-T. Takeda, J. Struct. Geol. 20, 1569 (1998).

375 [48] M. Thielmann, G.J. Golabek, and H. Marquardt, Geochemistry, Geophys. Geosystems 21, 1
376 (2020).

377 [49] Y. Wang, N. Hilairet, N. Nishiyama, N. Yahata, T. Tsuchiya, G. Morard, and G. Fiquet,
378 Geochemistry, Geophys. Geosystems 14, 3389 (2013).

379 [50] P. Kaercher, L. Miyagi, W. Kanitpanyacharoen, E. Zepeda-Alarcon, Y. Wang, F. De Carlo,
380 and H.-R. Wenk, Earth Planet. Sci. Lett. 456, 134 (2016).
381 [51] S. Speziale, J. Immoor, A. Ermakov, S. Merkel, H. Marquardt, and H.-P. Liermann, J.
382 Appl. Phys. 126, 105107 (2019).
383 [52] Y. Fei, A. Ricolleau, M. Frank, K. Mibe, G. Shen, and V. Prakapenka, Proc. Natl. Acad.
384 Sci. 104, 9182 (2007).
385 [53] S. Speziale, J. Immoor, A. Ermakov, S. Merkel, H. Marquardt, and H.-P. Liermann, J.
386 Appl. Phys. 126, 105107 (2019).

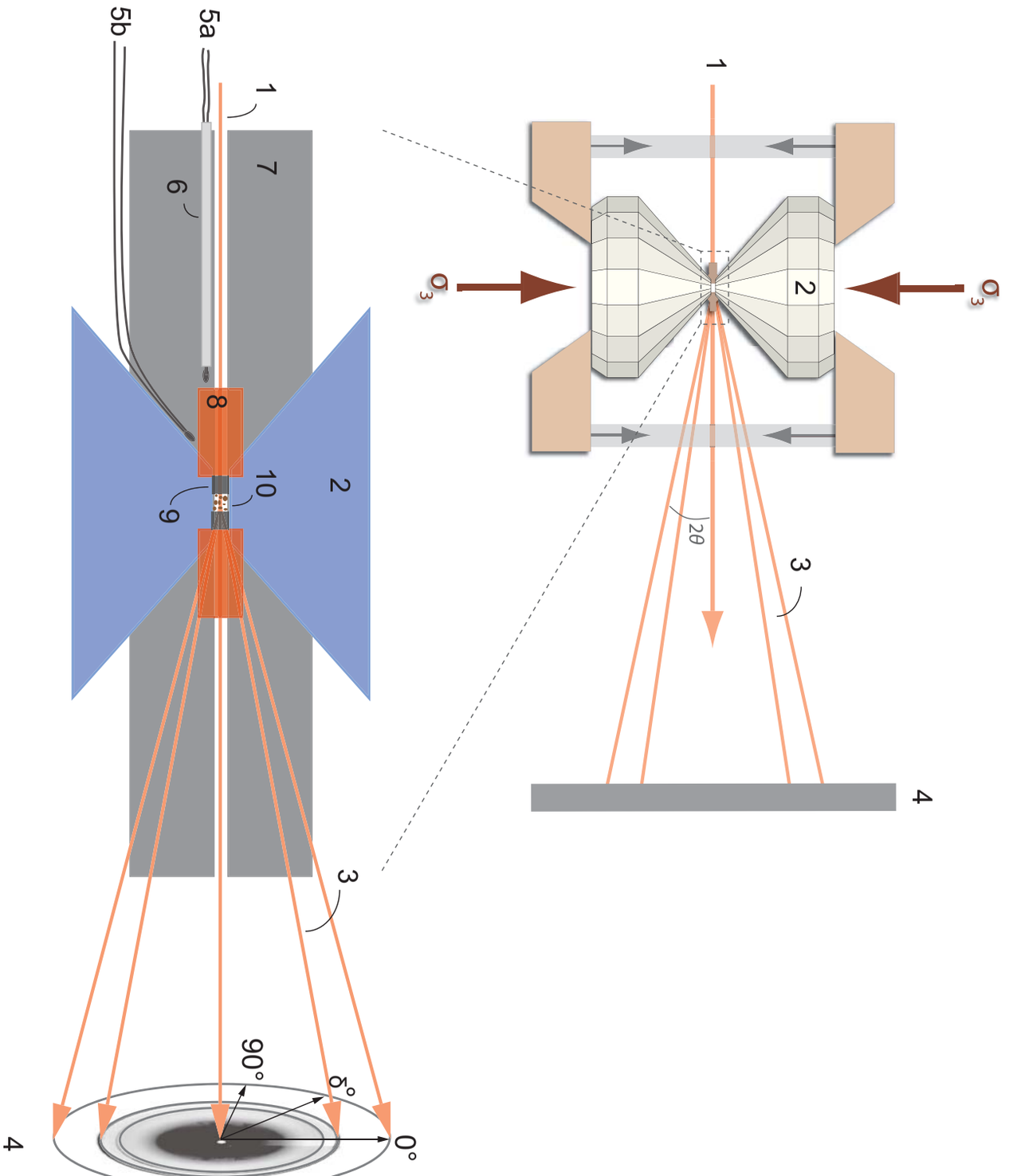

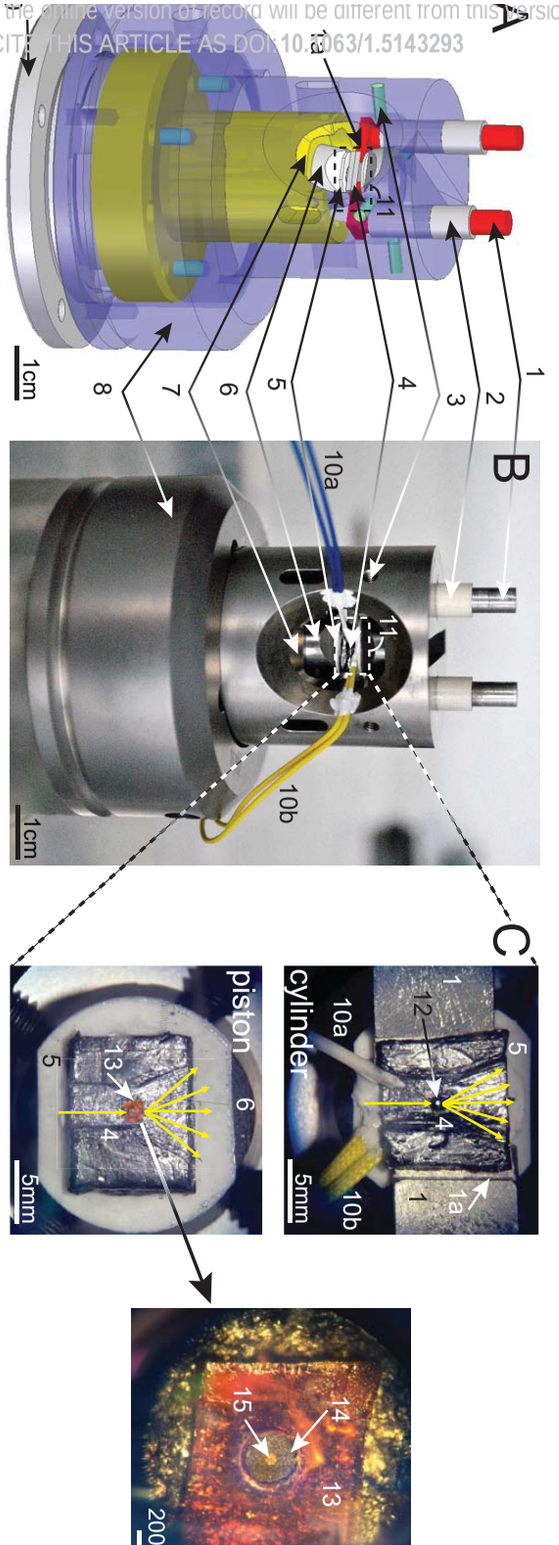

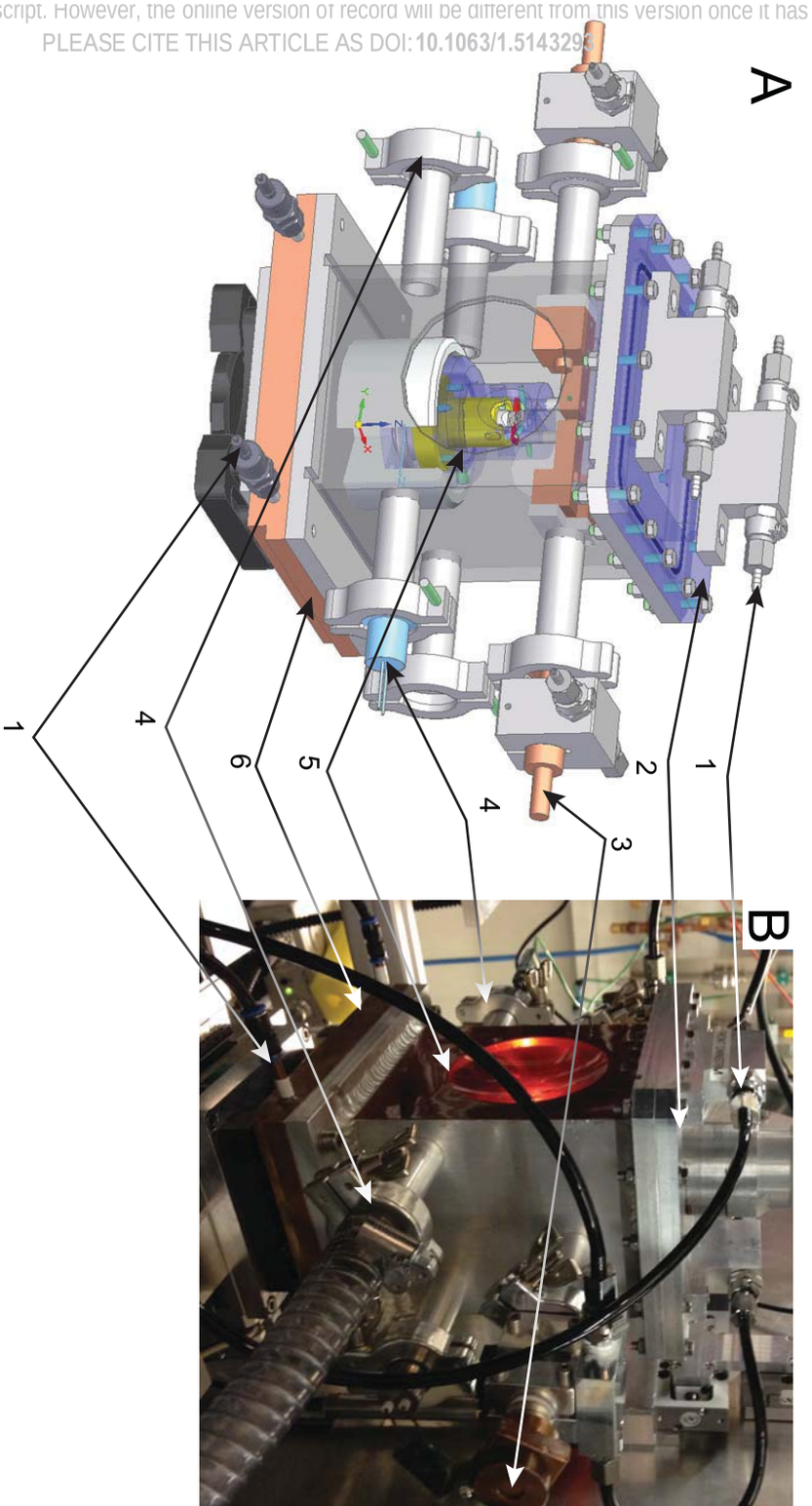

Review of Scientific Instruments

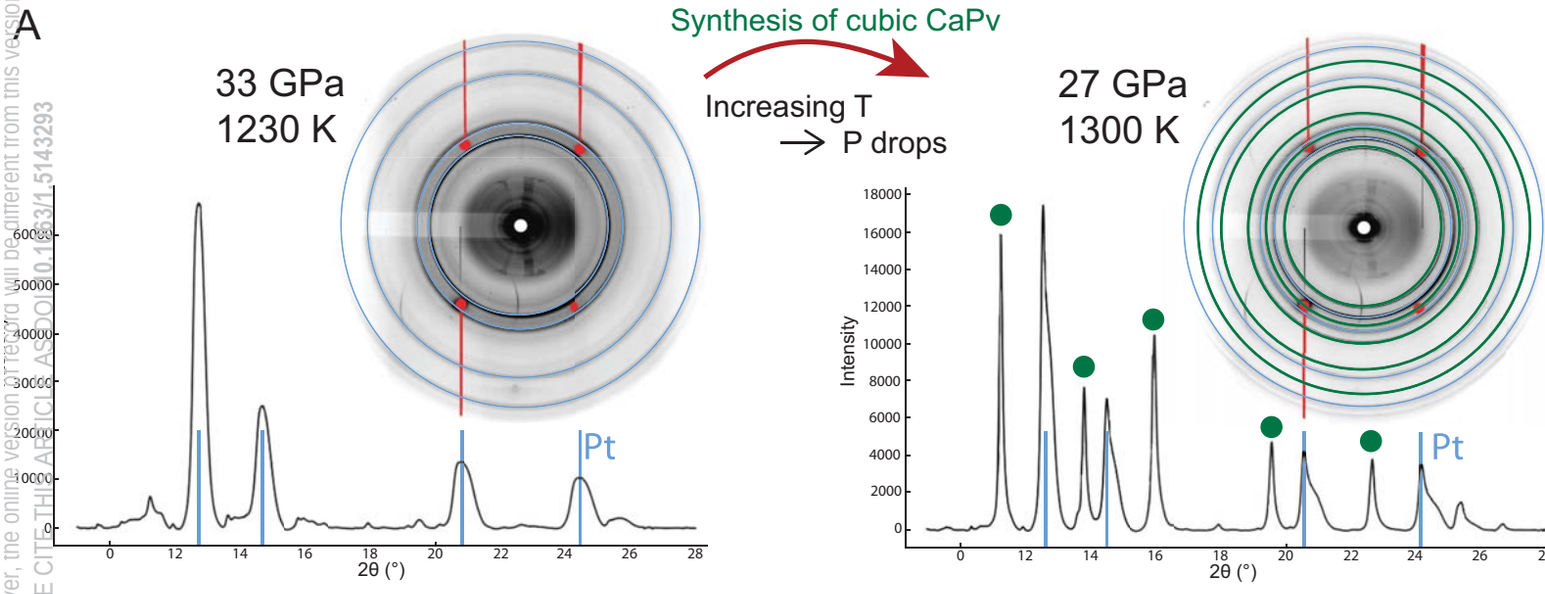

AIP Publishing

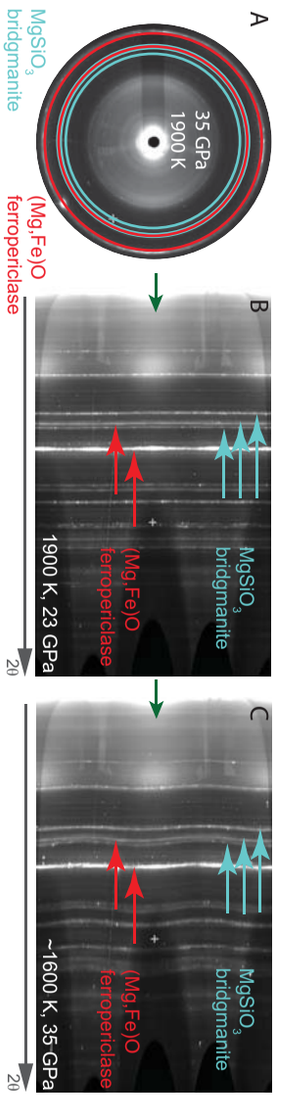

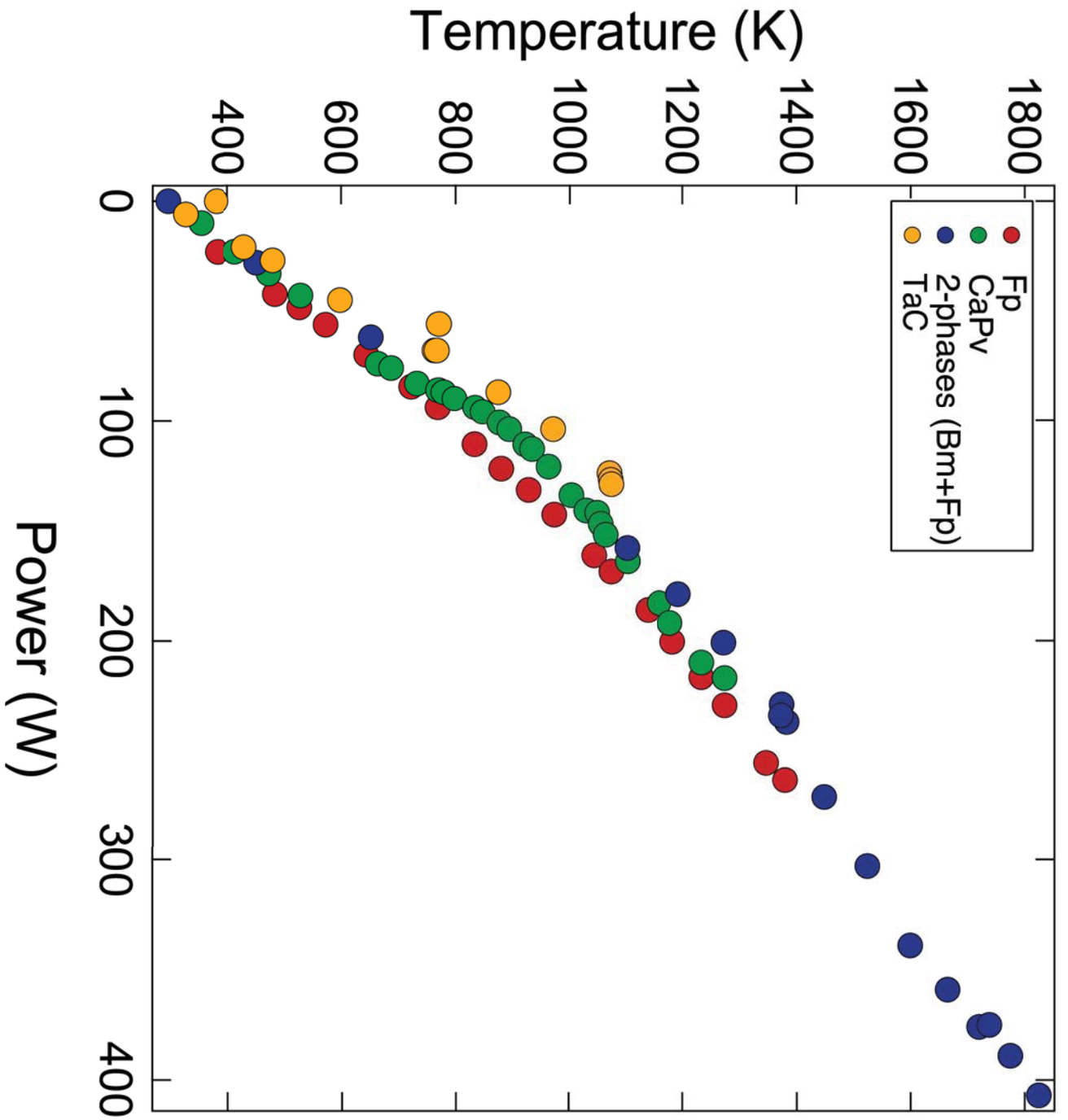

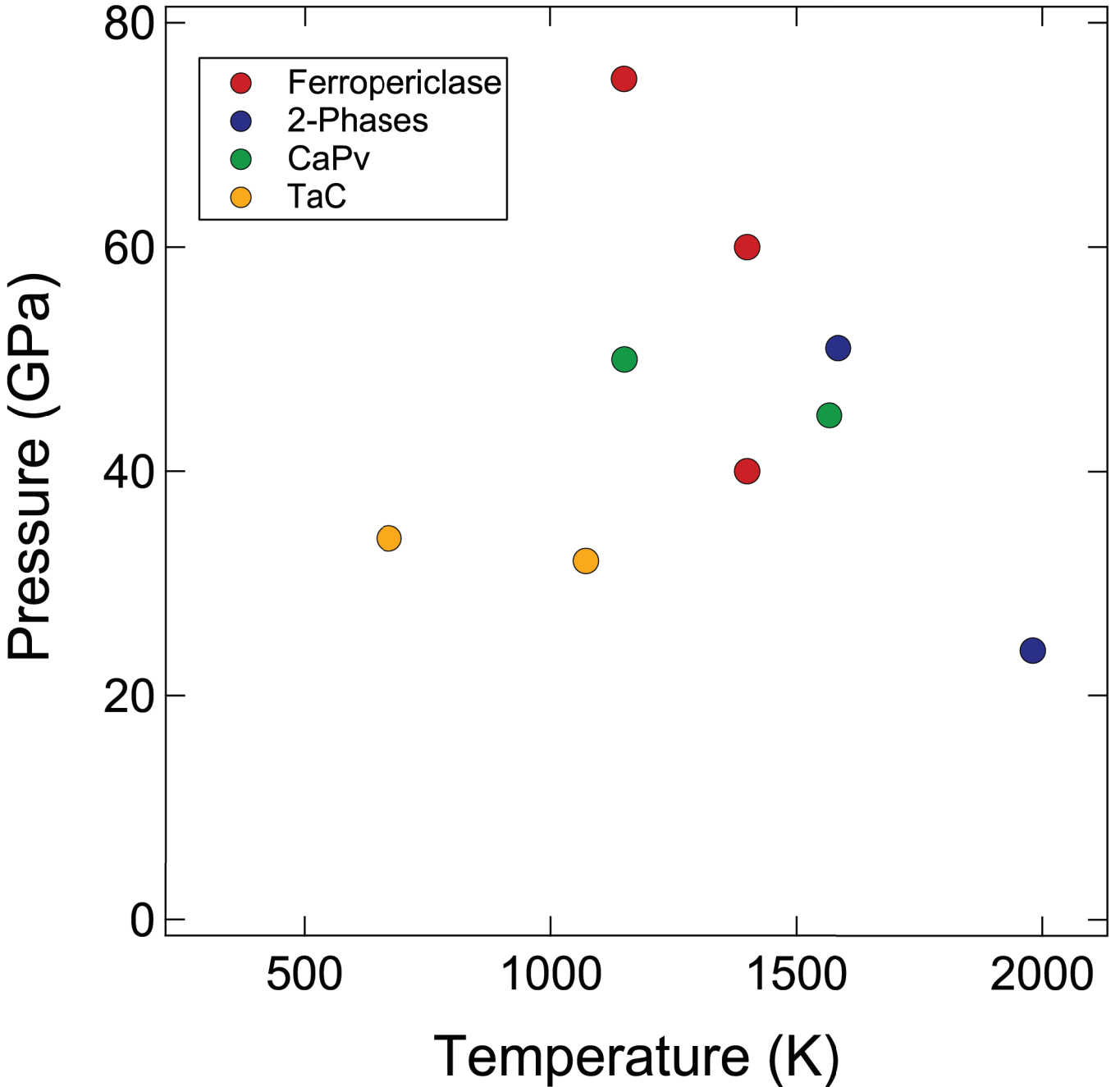
Ferropericlase
2-Phases
CaPv
TaC
Pressure (GPa)
Temperature (K)
0
20
40
60
80
500
1000
1500
2000